

# Experimental study on the cyclic behavior of reinforced concrete bridge piers with non-uniform corrosion

Jianfeng Zhao, Ying Lin, Xi Li<sup>\*</sup>, Qingyi Meng

School of Civil Engineering, Qingdao University of Technology, Qingdao 266033, China

## ARTICLE INFO

### Keywords:

Coastal bridge  
Non-uniform corrosion  
Cyclic load test  
Seismic performance  
Plastic hinge

## ABSTRACT

Coastal bridges exposed to the marine environment always suffer from non-uniform corrosion along the pier height. As the non-uniform corrosion increase, the material properties of the pier in the splash and tidal zone deteriorates significantly, affecting the seismic performance of the pier. In this study, four scaled bridge pier specimens were designed and fabricated. These specimens were subjected to different level of electrical accelerated corrosion in the proposed splash and tidal zone. Then, the cyclic load tests were conducted on the four bridge pier specimens. The hysteretic behavior, loading capacity, ductility, energy dissipation capacity and mean curvature of each specimen were analyzed. It was found that with increasing corrosion level, the load capacity, ductility and cumulative energy consumption of the specimens decreased. When the corrosion was severe enough, the location of the plastic hinge will transfer from the pier bottom to the corroded zone.

## 1. Introduction

In recent years, China has made a developmental leap in coastal bridge construction. However, the coastal bridges are usually exposed to harsh environments for significant periods of time. The problem of steel reinforcement corrosion caused by chloride penetration has become more prominent. The continuous chloride penetration will reduce reinforcement area [1], material strength [2,3], and bond between reinforcement and concrete [4]. Moreover, Due to most areas of China are at risk of earthquakes, coastal bridges may face a dual threat of harsh environmental conditions and earthquakes. Piers are the primary load-bearing members for bridge structures, and the severe deterioration of piers will reduce the seismic performance of coastal bridges [5]. To ensure the safety of coastal bridges, it is necessary to investigate the seismic performance of corroded piers and provide appropriate suggestions for the design and retrofit of coastal bridges [6].

At present, researchers have carried out a series of studies on the seismic performance of coastal bridges considering corrosion effects. For hysteretic behavior of corroded reinforced concrete (RC) columns, Ma et al. (2012) [7] conducted a cyclic loading tests on thirteen RC piers considering different corrosion degrees and axial load ratios. Meda et al. (2014) [8] evaluated the corrosion effect on strength and ductility reduction through cyclic loading tests of two full-scale column specimens. Guo et al. (2015) [9] investigated the corrosion effects on the

seismic performance of a coastal bridge during the long-term service period by cyclic experiment of four cantilever pier. Yang et al. (2016) [10] designed five groups of corroded RC columns with different maximum amounts of corrosion of rebar for testing the hysteretic behaviors. Goksu et al. (2016) [11] studied the seismic behavior of six RC columns which subjected different levels of accelerated corrosion process. Yuan and Fang et al. (2017) [12] carried a study on eight column specimens with different corrosion levels and repeated axial loadings under cyclic lateral loads. Di Carlo et al. (2017) [13] studied the behavior of corroded columns under cyclic loads with a three-dimensional finite element analysis considering interface decay and buckling effects. Rajput et al. (2018) [14] casted six real size specimens to examine the effects of corrosion on RC columns. Li et al. (2018) [15] carried out a pseudo-dynamic test on six corroded square RC columns with different axial compression ratios and corrosion levels to study influence of non-uniform corrosion of steel bars on the seismic behavior of RC columns. Yalciner et al. (2020) [16] tested a total of 30 full-scale RC columns to develop models for the prediction of the structural behavior of corroded RC columns. Dai et al. (2020) [17] experimentally studied the seismic behavior of corroded RC columns with a focus on the comparison between two different accelerated corrosion techniques by using artificial climate environment (ACE) and electrochemical chloride extraction (ECE). These research results show that the seismic performance of bridge piers is strongly affected by the corrosion, and as the

<sup>\*</sup> Corresponding author.

E-mail address: [xi.li@qut.edu.cn](mailto:xi.li@qut.edu.cn) (X. Li).

<https://doi.org/10.1016/j.istruc.2021.04.060>

Received 14 October 2020; Received in revised form 31 March 2021; Accepted 21 April 2021

Available online 14 May 2021

2352-0124/© 2021 Institution of Structural Engineers. Published by Elsevier Ltd. All rights reserved.

**Table 1**  
Similitude relation in this study.

Type	Physical quantity	Similitude parameter
Geometric and material properties	Length	1/8
	Area	1/64
	Linear displacement	1/8
	Angular displacement	1
	Strain	1
Reinforcement ratio	Stress	1
	Elastic modulus	1
	Longitudinal reinforcement	1
	Stirrup	1

corrosion degree increases, loading capacity, stiffness, energy dissipation and ductility decrease.

For seismic evaluation methodology of corroded RC columns, Ou et al. (2013)[18] presented a new seismic evaluation methodology for corroded reinforced concrete bridge on the basis of nonlinear static pushover analysis. Biondini et al. (2014)[19] proposed a probabilistic approach to predict the lifetime seismic performance of concrete bridges exposed to corrosion based on nonlinear static pushover analysis. Akiyama et al. (2014)[20] presented a novel computational procedure to integrate the probabilistic hazard associated with airborne chlorides into life-cycle seismic reliability of bridge piers. Guo et al. (2015)[21] developed a new deterministic corrosion rate model to assess the time-variant seismic performance of corroding RC bridge columns. Asgh-shahr et al. (2018)[22] presented a study of the time-dependent seismic performance of RC bridges and proposed a new framework for pushover analysis. Cui et al. (2018)[23] presented an improved reinforced concrete steel bar deterioration model that incorporates pitting corrosion and considers the change in after-cracking corrosion rate to assess the time-dependent seismic fragility of RC bridge substructures in marine environments. Li et al. (2020)[24] proposed an alternative time-dependent seismic fragility assessment framework considering the variable correlation of structural random parameters for aging highway bridges subject to non-uniform chloride-induced corrosion attacks.

For seismic retrofitting of corroded RC columns, Rajput et al. (2019)[25] carried out a comprehensive study to develop retrofitting scheme for restoring the structural performance of corroded confined concrete hinge regions of RC columns by using advanced composite materials. Yu et al. (2020)[26] presented a life cycle embodied energy assessment (LCEEA) framework for a typical RC structures in seismic regions. Jia et al. (2020)[27] tested three 1/4-scaled RC column with and without retrofit by carbon fiber reinforced polymer (CFRP) fabric in order to investigate seismic performance of low-level corroded columns and the efficiency of CFRP as a retrofit measure.

The previously mentioned studies on the seismic performance of corroded bridge structures have made meaningful advancements in this field of research. Besides, it is widely recognized that steel reinforcements of the bridge piers in the splash and tidal zone were more severely corroded than in atmospheric and submerged zone owing to higher surface chloride concentration, oxygen abundance and wet-drying cyclic. Yuan and Guo (2018, 2020)[28–31] investigated the seismic performance of non-uniform corroded bridge piers by cyclic load and shake table test considering the effect of biaxial earthquake excitation, bond-slip. The results indicated that the seismic-resistance capacity of the splash and tidal zone is significantly lower than the pier bottom when corrosion was severe. This phenomenon will cause the location of the plastic hinge of the bridge pier to change when subjected earthquake. Comparing with inland bridges which plastic hinges usually appear at the bottom of piers, the location of plastic hinges of the coastal bridges may be found at the corrosion zone of the piers. Due to rarely previous studies regarding this issue before, it is necessary to conduct a more in-depth research on the seismic performance of bridge piers with

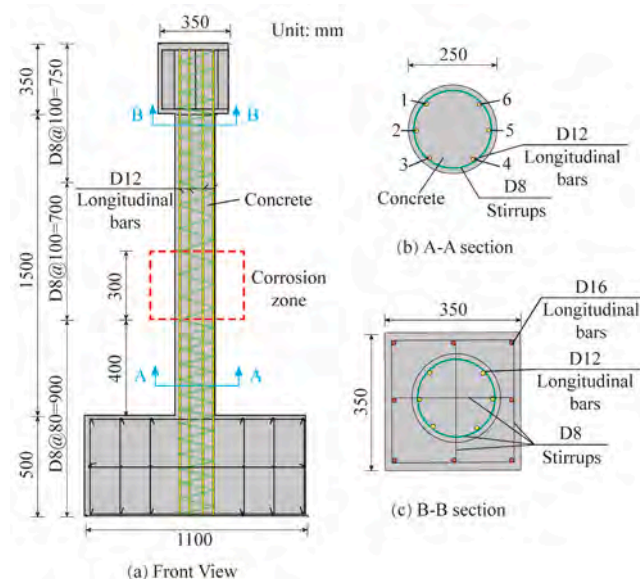


**Fig. 1.** Specimen geometry and reinforcement details.

non-uniform corrosion. Therefore, in order to clarify the effect of non-uniform corrosion on coastal bridge piers, cyclic loading test of four scaled bridge piers was conducted in this study.

## 2. Experimental program

### 2.1. Specimen details

Four scaled models of RC piers with different corrosion degrees (0%, 10%, 20% and 30%) were constructed. The similitude relation of this study is given in Table 1. The dimensions, materials, reinforcement arrangement and vertical load of the four bridge pier models are same, and the details are shown in Fig. 1. The specimens were all made with C30 concrete. The longitudinal reinforcements and stirrups were HRB400 steel with a diameter of 12 mm and HRB335 steel with a diameter of 8 mm, respectively. The longitudinal reinforcement ratio was 1.38%, and the stirrup form is the same as the prototype structure. The spacing of the stirrups in the encrypted region and the non-encrypted region was 80 mm and 100 mm, respectively. According to Chinese test standard[32,33], the mechanical property tests for concrete and reinforcements were carried out. The compressive strength of the concrete at an age of 28 days was tested to be 31.6 MPa. The yield and ultimate strength of the longitudinal reinforcements was tested to be 432.65 MPa and 667.43 MPa, respectively. The corresponding values for the stirrups was 367.28 MPa and 546.52Mpa, respectively.

### 2.2. Electrical accelerated corrosion

Due to the large size of the test models and the requirement of localized corrosion, the electrical accelerated corrosion method was selected to corrode the test models to varying degrees. The proposed corrosion zone was selected to be 400 to 700 mm from the pier bottom, which represents the splash and tidal zone in the actual marine environment. The test cycles, swell cracks, and corrosion products generated by the electrical accelerated corrosion were chosen to be similar to the rusted bridge specimens under natural conditions. Maaddawy and Soudki [34] suggested to control the corrosion current density of the test specimens in the range of 100 ~ 550  $\mu\text{A}/\text{cm}^2$ . Therefore, the corrosion current density of the electrical accelerated corrosion test for this study was selected as 300  $\mu\text{A}/\text{cm}^2$ , and the target corrosion rates of the three test specimens was 10%, 20%, and 30%, respectively. According to Faraday’s electrolysis law, the energization time of each test specimens

**Table 2**  
Energization time of each test specimen.

Specimen	Target corroded rates	Corrosion current density( $\mu\text{A}/\text{cm}^2$ )	Current intensity(A)	Energization time(h)
D1	10%	300	0.46	562.6
D2	20%	300	0.46	1125.84
D3	30%	300	0.46	1687.68

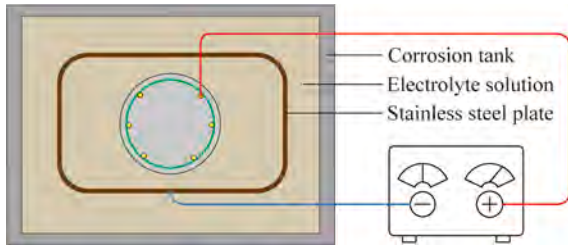


Fig. 2. Diagram of the electrical accelerated corrosion circuit.



Fig. 3. Actual corrosion of the test specimens.

was calculated as list in Table 2. The test specimens that corroded to the degree of 0%, 10%, 20%, and 30% was named D0, D1, D2, and D3, respectively.

The schematic diagram of the electrical accelerated corrosion circuit is shown as Fig. 2. In electrical accelerated corrosion test, a 5% NaCl solution was used as the electrolyte solution, and a stainless-steel plate

was used as the cathode. A DC steady current power supply provided a constant current of 0.46A. The actual corrosion of the specimens is shown as Fig. 3.

2.3. Experimental setup and loading protocol

Fig. 4 shows the experimental setup of loading test. As shown in Fig. 4, the foundation of the test model was anchored to the rigid floor by four threaded rods. During the experiment, all the test models were loaded under a constant axial compression and a cyclic lateral displacement with increasing amplitude. The constant vertical axial load applied by the hydraulic jack was 310 kN and the corresponding axial compression ratio was 0.2. The unilateral cyclic displacement loads were applied by a horizontal MTS actuator and increased by 4 mm at each loading level as shown in Fig. 5. The experiment was stopped when the lateral resistance force dropped to less than 85% of the peak load.

As shown in Fig. 4(a), two LVDTs were used to directly capture the lateral displacement at the top and bottom of the pier models. Meanwhile, the two LVDTs can be also used to check the actual displacement output by the actuator and the slip between the pier foundation and the rigid floor. Moreover, to observe the transfer of plastic hinge, the curvature of the section of the pier bottom and the end sections of the corrosion zone were measured by installing three pairs of LVDTs at the heights of 100 mm, 400 mm and 700 mm above the pier bottom.

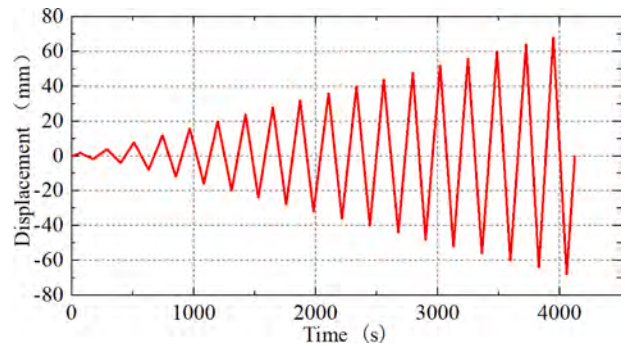
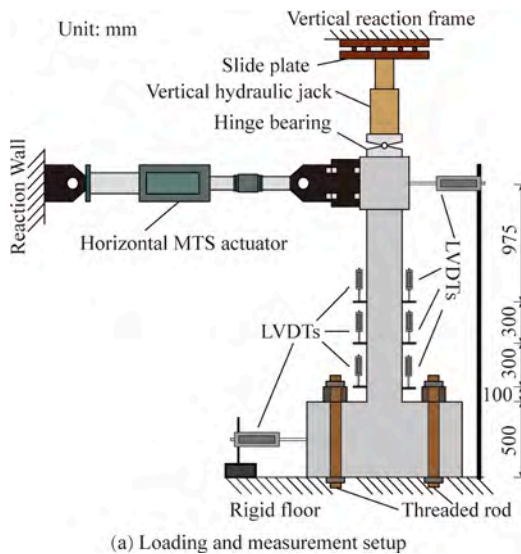


Fig. 5. Unilateral loading history.



(a) Loading and measurement setup

(b) Actual test model

Fig. 4. Experimental setup.

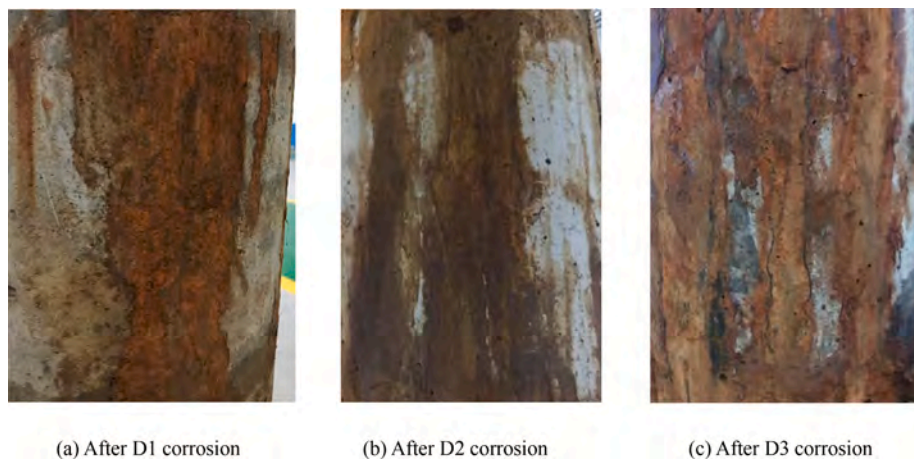


Fig. 6. Surface condition of concrete after corrosion.



Fig. 7. Images of the concrete reinforcement after varying degrees of corrosion.

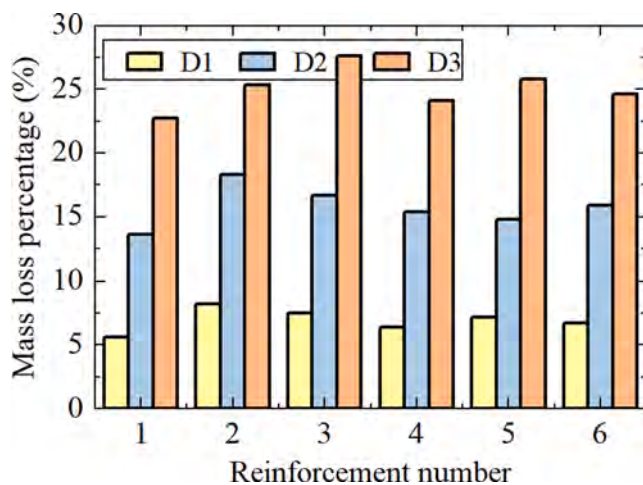


Fig. 8. Mass loss percentage of each reinforcement.

### 3. Experimental results

#### 3.1. Experimental observation

Fig. 6 shows the corrosion state of the concrete surface for specimen D1, D2 and D3, respectively. It can be observed that with the increase of

Table 3

Average mass loss percentage.

	D1	D2	D3
Average mass loss percentage (%)	6.93	15.78	25.02
Difference from target corrosion rate (%)	3.07	4.22	4.98

corrosion degree, the surface rust on the specimens increased significantly. The specimen D3 had the worst corrosion, and the gradual accumulation of rust products causes the rust layer to expand around the longitudinal reinforcements. For some pier models, the concrete cover in corrosion zone formed vertical swell cracks (Fig. 6 (c)). In addition, yellow–brown rust marks were visible around the cracks.

In order to assess the actual degree of reinforcement corrosion, longitudinal reinforcements in the corrosion zones were stripped from the concrete after the test as shown in Fig. 7. After a series of cleaning procedures, the mass loss percentage of each reinforcement was calculated and presented in Fig. 8. In this figure, the longitudinal reinforcements were assigned a unique number as shown in Fig. 1(b). The average mass loss percentage of the specimens were tabulated in Table 3. It can be seen that although the actual corrosion rate of the specimens did not reach the target corrosion rate, the relatively ideal corrosion specimens were also obtained.

Fig. 9 shows the crack morphology and failure mode of the four specimens after the cyclic loading test. All specimens behaved linearly within the lateral displacement of 8 mm, and as the loading progressed,



Fig. 9. Specimen appearance after the cyclic test.

the cracks first occurred at the pier bottom. The damage at corrosion specimens was more extensive than that at the un-corrosion specimens. For the specimen without corrosion (Specimen D0), the cracks gradually extended upward from the pier bottom with the loading increase. The cracks were mainly distributed in the range of 800 mm above the pier bottom after the final displacement was reached at 68 mm, as shown in Fig. 9(a). For the specimens with corrosion (Specimen D1, D2 and D3), when the lateral displacement was close to 44 mm, the concrete cover had already been spalled off as shown in Fig. 9(b)–(d). Due to the slight corrosion level of Specimen D1, the failure mode and the location of cracks and concrete cover spalling were both similar with Specimen D0. However, with the increase of corrosion, concrete cover started to spall off in the corrosion zone, especially for the case of Specimen D3. As for Specimen D3, large area of concrete cover in the corrosion zone had already been spalled off and some longitudinal reinforcements were exposed. Due to the effect of corrosion, the loading capacity of the corrosion zone was reduced, which lead to the location of the plastic hinge transfer from the pier bottom to the splash and tidal zone. This phenomenon indicating that the corrosion in the splash and tidal zone began to affect the failure mode of the pier.

### 3.2. Hysteretic curves

Fig. 10 shows load–displacement hysteretic loop of the four specimens, which representing the relationship between the lateral force and relative displacement of the pier model during the cyclic test. Specimen D0 was loaded up to the displacement of 68 mm, while the corroded specimens were loaded up to the lateral displacement of 47 mm, 44 mm, 40 mm, respectively for Specimen D1 to D3. As the corrosion level of the specimen increased, the area enclosed by hysteretic loop decreased and the pinching effect became more obvious. It means that the energy dissipation capacity of the pier was degraded. Compared with the uncorroded specimen, the final displacements applied to each specimen decreased by 23.5%, 35.3%, and 41.2%, respectively. It is indicated that

the seismic performance of the specimen decreases as the corrosion becomes serious.

### 3.3. Lateral resistance capacity and ductility

Skeleton curves are the curves linking the peak loads at each load level in positive and negative directions, demonstrating that the differences in load capacity and ductility. Fig. 11 shows the skeleton curves of the four specimens. Compared with specimen D0, the peak lateral forces of Specimen D1, D2, and D3 were significantly reduced. Table 4 summarizes key parameters at the skeleton curves of all specimens. The key parameters are yielding load ( $F_y$ ), yielding displacement ( $D_y$ ), peak load ( $F_{max}$ ), peak displacement ( $D_{max}$ ), ultimate load ( $F_u$ ), ultimate displacement ( $D_u$ ) and ductility factor ( $\mu$ ) respectively. The yielding load and displacement are obtained based on the principle of equivalent energy. The ultimate load and displacement respectively represents the load and corresponding displacement when the lateral resistance force drop to 85% of the peak load.

As list in Table 4, compared with specimen D0, the peak loads of Specimen D1, D2, and D3 decreased by 8%, 17.1%, and 23.3% respectively, from 25.7kN of Specimen D0 to 19.7kN of Specimen D3. Moreover, as the corrosion increases, the ductility factor of the specimen continued to decrease from 4 of Specimen D0 to 2.2 of Specimen D3, with the decrease of 45%. It is obvious that both the lateral resistance capacity and the ductility of corroded bridge piers were reduced significantly compared to uncorroded bridge piers. it is indicated that when the bridge pier experience corrosion during the service life, their seismic performance will decline gradually.

### 3.4. Energy dissipation

The cumulative energy consumption is obtained by calculating the area of the hysteresis loop as shown in Fig. 12. When the displacement applied to each specimen was less than 20 mm, the corrosion effect on

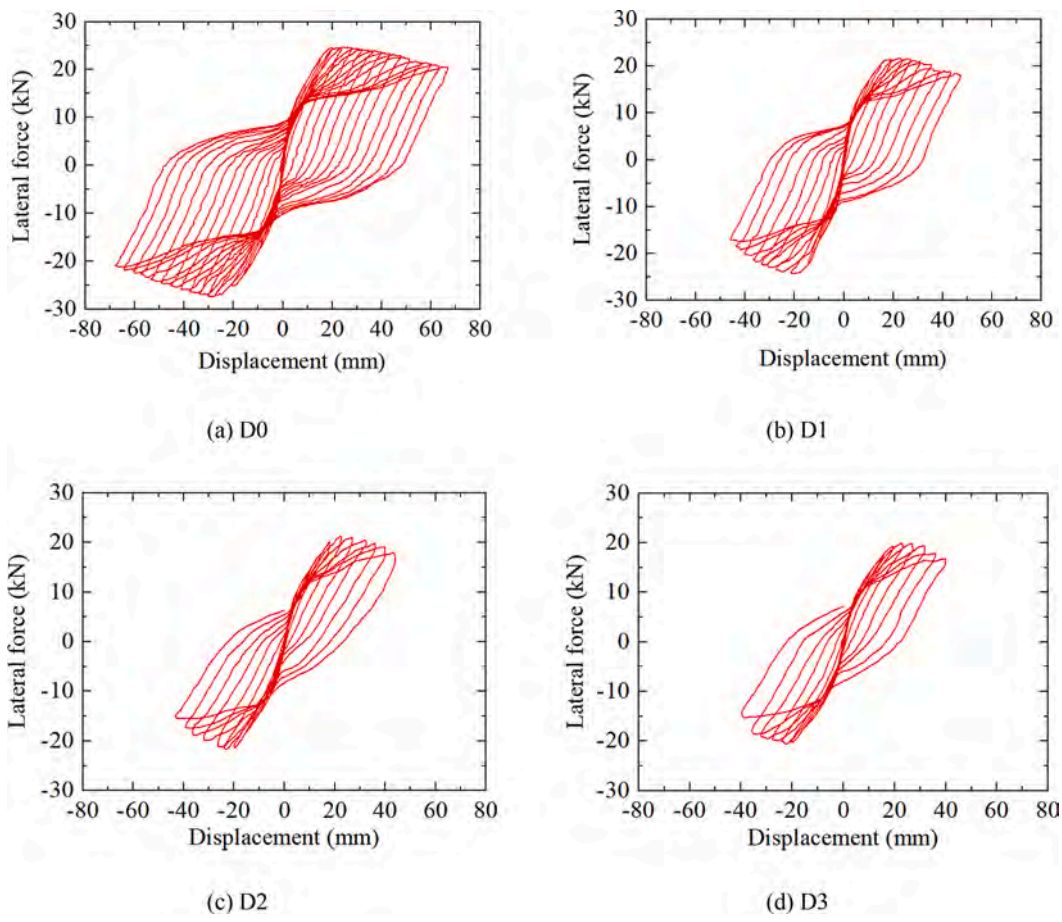


Fig. 10. Test hysteresis curves.

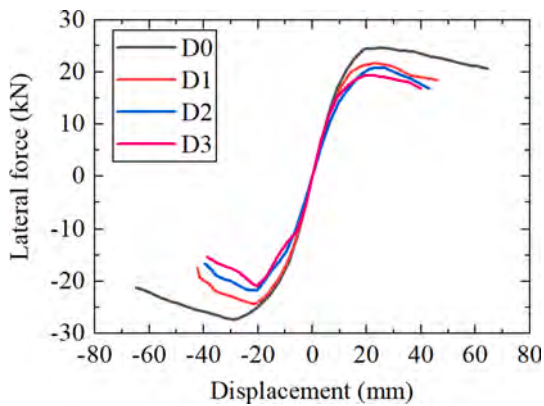


Fig. 11. Skeleton curves.

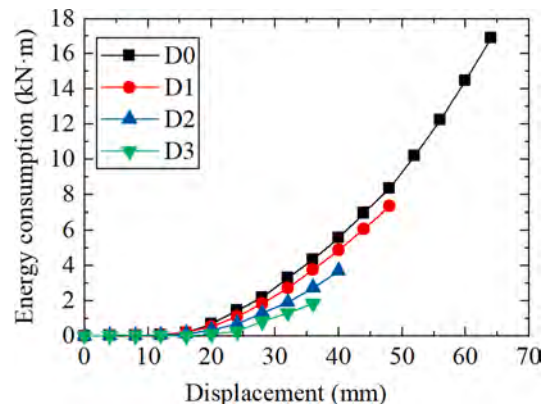


Fig. 12. Cumulative energy consumption.

**Table 4**  
Key parameters in skeleton curves.

Load direction	specimen	Yielding point		Peak point		Ultimate point		Ductility factor
		Disp. (mm)	Load (kN)	Disp. (mm)	Load (kN)	Disp. (mm)	Load (kN)	
Positive direction	D0	16.7	19.3	19.0	26.4	67.6	22.4	4.0
	D1	16.0	21.9	20.8	22.5	48.6	19.1	3.0
	D2	17.9	22.3	22.0	21.7	44.5	18.4	2.5
	D3	16.7	18.5	19.4	17.8	37.4	15.1	2.2
Negative direction	D0	16.1	21.7	27.2	25.0	63.8	21.3	4.0
	D1	17.2	21.3	19.8	24.7	47.8	21.0	2.8
	D2	16.7	20.9	23.2	20.9	43.3	17.8	2.6
	D3	16.2	17.1	19.2	21.6	36.2	18.4	2.2

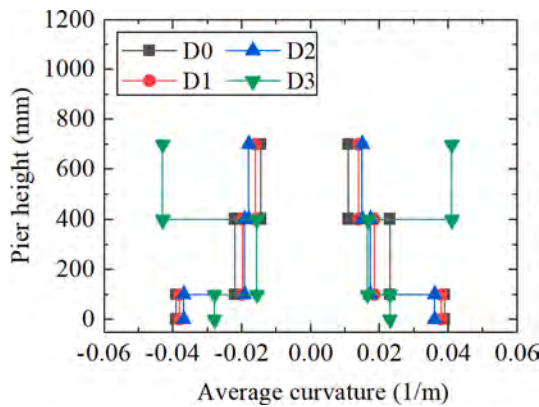


Fig. 13. Average curvature distribution.

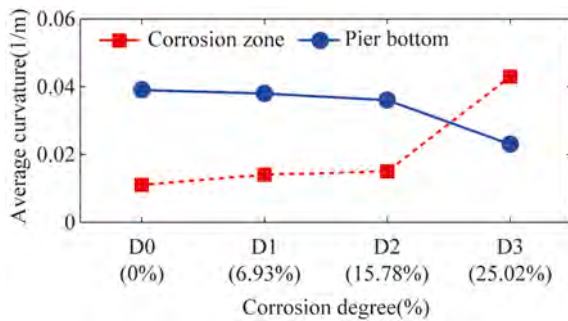


Fig. 14. Relation of Average curvature and corrosion degree.

energy consumption was not vary obviously, which was due to the small nonlinear deformation of the structure. When the applied displacement exceeded 20 mm, the difference of the cumulative energy consumption of each specimen gradually increased. The energy consumption of each specimen increased with the nonlinear deformation. At the same displacement, the cumulative energy consumption value of the specimen decreased with the increasing corrosion level.

### 3.5. Curvature

Due to the limit load displacement of the Specimen D3, the curvature of each specimen was obtained at the displacement of  $\pm 36.8$  mm, as shown in Fig. 13. For the uncorroded (0%) Specimen D0, the slight corroded (6.93%) Specimen D1 and the medium corroded (15.78%) Specimen D2, the maximum average curvature appeared in the region of 0 ~ 100 mm above the pier bottom which was the normal position of the plastic hinge of the bridge piers. For the sever corroded (25.02%) Specimen D3, the maximum average curvature was found at the corrosion zone which was 400 ~ 700 mm above the pier bottom. It means that the position of plastic hinge had changed to the corrosion zone. The similar phenomenon was also obtained by Yuan (2017)[28] and further verified by this study. Moreover, although the steel strength of the test models in this study was different from that in previous study of Yuan (2017)[28], the transfer of plastic hinge still be observed when the corrosion was severe (25.02% for this study and 17.59% for Yuan (2017) [28]).

To further verify the relation between the curvature distribution and the corrosion degree, the average curvature of pier bottom and corrosion zone were analyzed and shown in Fig. 14. As seen from the figure, the average curvature of the pier bottom decreased with the corrosion degree increased, but the average curvature of corrosion zone exhibited a opposite trend. For Specimen D0 ~ D2 (corrosion degree 0%, 6.93% and 15.78%, respectively), the average curvatures of pier bottom were

0.039, 0.038 and 0.036 1/m respectively while the average curvatures of corrosion zone were 0.011, 0.014 and 0.015 1/m respectively. The average curvatures of corrosion zone were obviously smaller than the ones of pier bottom. Therefore, it can be concluded that the plastic hinges only occurred at the pier bottom, which consisted with the experimental observation as show in Fig. 9(a)~(c). For Specimen D3 (corrosion degree 25.02%), the average curvature of pier bottom was 0.023 1/m while the average curvature of corrosion zone was 0.043 1/m. The average curvature of corrosion zone was obviously larger than the one of pier bottom, so it can be concluded that the plastic hinge transferred to the corrosion zone, which also consisted with the experimental observation as show in Fig. 9(d).

These observations demonstrate that (1) even if the moment in the corrosion region was less than the one at the pier bottom, the load capacity of corrosion region was significantly reduced by the material performance degradation, (2) the position of plastic hinge will be changed to the corrosion zone when the corrosion was severe, and (3) the transfer of plastic hinge will not be affected by material strength. As a result, more attention should be paid to the change of the failure mode of the pier and the position of plastic hinge when the corrosion is severe.

## 4. Conclusions

This study considers the non-uniform corrosion of coastal bridge piers. Four pier specimens with different corrosion levels in the proposed corrosion zone were designed and cyclic load test was performed. Based on the test results, the main conclusions are as follows:

- (1) Three bridge pier specimens were corroded using the electrical accelerated corrosion test. Comparing the actual average mass loss percentage of the reinforcements of each specimen with the target corrosion rate, the electric accelerated corrosion test can obtain relatively ideal test corrosion rate.
- (2) Comparing with the uncorroded specimen, the corroded specimens showed a poor hysteresis performance, of which the peak load decreased by up to 23.3% while the ductility down to 45% and the accumulated energy consumption decreased from 16.9kN-m to 1.8kN-m.
- (3) The seismic failure mode of the coastal bridges will be changed caused by the material performance degradation in corrosion zone. The position of plastic hinge will transfer from the pier bottom to the corrosion zone when the corrosion was severe, and the transfer of plastic hinge will not be affected by material strength.

It should be noted, Due to the constitutive model of corroded reinforcements and the interaction between corroded reinforcements and concrete cannot be verified in this study, numerical analysis on the corroded bridge piers was not carried out, but it will be presented in a future work.

### Declaration of Competing Interest

The authors declare that they have no known competing financial interests or personal relationships that could have appeared to influence the work reported in this paper.

### Acknowledgment

This work was supported by National Natural Science Foundation of China (Grant No. 51778314 and Grant No. 51508473), Sichuan Science and Technology Program (2019YJ0239).

## References

- [1] Andrade C, Alonso C, Molina FJ. Cover cracking as a function of bar corrosion: Part I-Experimental test. *Materials and Structures*; 1993. p. 26453–64.
- [2] Coronelli D, Gambarova P. Structural assessment of corroded reinforced concrete beams: Modeling guidelines. *J Struct Eng* 2004;1301214–24.
- [3] Kashani MM, Crewe AJ, Alexander NA. Nonlinear cyclic response of corrosion-damaged reinforcing bars with the effect of buckling. *Constr Build Mater* 2013; 41388–400.
- [4] Choi YS, Yi S, Kim MY, Jung WY, Yang EI. Effect of corrosion method of the reinforcing bar on bond characteristics in reinforced concrete specimens. *Constr Build Mater* 2014;54180–9.
- [5] Deng P, Zhang C, Pei S, Jin Z. Modeling the impact of corrosion on seismic performance of multi-span simply-supported bridges. *Constr Build Mater* 2018; 185193–205.
- [6] Alipour A, Shafei B, Shinozuka M. Performance evaluation of deteriorating highway bridges located in high seismic areas. *J Bridge Eng* 2011;16597–611.
- [7] Ma Y, Che Y, Gong J. Behavior of corrosion damaged circular reinforced concrete columns under cyclic loading. *Constr Build Mater* 2012;29548–56.
- [8] Meda A, Mostosi S, Rinaldi Z, Riva P. Experimental evaluation of the corrosion influence on the cyclic behaviour of RC columns. *Eng Struct* 2014;76112–23.
- [9] Guo A, Li H, Ba X, Guan X, Li H. Experimental investigation on the cyclic performance of reinforced concrete piers with chloride-induced corrosion in marine environment. *Eng Struct* 2015;1051–11.
- [10] Yang S, Song X, Jia H, Chen X, Liu X. Experimental research on hysteretic behaviors of corroded reinforced concrete columns with different maximum amounts of corrosion of rebar. *Constr Build Mater* 2016;121319–27.
- [11] Goksu C, Ilki A. Seismic behavior of reinforced concrete columns with corroded deformed reinforcing bars. *ACI Struct J* 2016;1131053–64.
- [12] Yuan Z, Fang C, Parsaeimaram M, Yang S. Cyclic behavior of corroded reinforced concrete bridge piers. *J Bridge Eng* 2017;22.
- [13] Di Carlo F, Meda A, Rinaldi Z. Numerical evaluation of the corrosion influence on the cyclic behaviour of RC columns. *Eng Struct* 2017;153264–78.
- [14] Rajput AS, Sharma UK. Corroded reinforced concrete columns under simulated seismic loading. *Eng Struct* 2018;171453–63.
- [15] Li D, Wei R, Xing F, Sui L, Zhou Y, Wang W. Influence of Non-uniform corrosion of steel bars on the seismic behavior of reinforced concrete columns. *Constr Build Mater* 2018;16720–32.
- [16] Yalciner H, Kumbasaroglu A. Experimental evaluation and modeling of corroded reinforced concrete columns. *ACI Struct J* 2020;11761–76.
- [17] Dai K, Liu C, Lu D, Yu X. Experimental investigation on seismic behavior of corroded RC columns under artificial climate environment and electrochemical chloride extraction: A comparative study. *Constr Build Mater* 2020;242.
- [18] Ou Y, Fan H, Nguyen DN. Long-term seismic performance of reinforced concrete bridges under steel reinforcement corrosion due to chloride attack. *Earthquake Eng Struct Dyn* 2013;422113–27.
- [19] Biondini F, Camnasio E, Palermo A. Lifetime seismic performance of concrete bridges exposed to corrosion. *Struct Infrastruct Eng* 2014;10880–900.
- [20] Akiyama M, Frangopol DM. Long-term seismic performance of RC structures in an aggressive environment: Emphasis on bridge piers. *Struct Infrastruct Eng* 2014; 10865–79.
- [21] Guo Y, Trejo D, Yim S. New model for estimating the Time-Variant seismic performance of corroding RC bridge columns. *J Struct Eng* 2015;141.
- [22] Asghshahr MS, Rahai A. Seismic assessment of reinforced concrete bridge under Chloride-Induced corrosion. *International Journal of Civil Engineering*. 2018: 16681–93.
- [23] Cui F, Zhang H, Ghosn M, Xu Y. Seismic fragility analysis of deteriorating RC bridge substructures subject to marine chloride-induced corrosion. *Eng Struct* 2018;15561–72.
- [24] Li H, Li L, Zhou G, Xu L. Time-dependent seismic fragility assessment for aging highway bridges subject to non-uniform chloride-induced corrosion. *J Earthquake Eng* 2020.
- [25] Rajput AS, Sharma UK, Engineer K. Seismic retrofitting of corroded RC columns using advanced composite materials. *Eng Struct* 2019;18135–46.
- [26] Yu R, Chen L, Zhang D, Wang Z. Life cycle embodied energy analysis of RC structures considering chloride-induced corrosion in seismic regions. *Structures*. 2020;25839–48.
- [27] Jia J, Zhao L, Wu S, Wang X, Bai Y, Wei Y. Experimental investigation on the seismic performance of low-level corroded and retrofitted reinforced concrete bridge columns with CFRP fabric. *Eng Struct* 2020;209.
- [28] Yuan W, Guo A, Li H. Experimental investigation on the cyclic behaviors of corroded coastal bridge piers with transfer of plastic hinge due to non-uniform corrosion. *Soil Dyn Earthquake Eng* 2017;102112–23.
- [29] Yuan W, Guo A, Yuan W, Li H. Shaking table tests of coastal bridge piers with different levels of corrosion damage caused by chloride penetration. *Constr Build Mater* 2018;173160–71.
- [30] Yuan W, Guo A, Yuan W, Li H. Experimental investigation on cyclic behavior of coastal bridge piers with non-uniform corrosion under biaxial quasi-static loads. *Constr Build Mater* 2018;190222–34.
- [31] Yuan W, Guo A, Li H. Equivalent elastic modulus of reinforcement to consider bond-slip effects of coastal bridge piers with non-uniform corrosion. *Eng Struct* 2020;210.
- [32] CISA. Test methods of steel for reinforcement of concrete. GB/T 28900-20122012.
- [33] MOHURD. Standard for test methods of concrete physical and mechanical properties. GB/T 50081-20192019.
- [34] Maaddawy TAE, Soudki KA. Effectiveness of impressed current technique to simulate corrosion of steel reinforcement in concrete. *J Mater Civ Eng* 2003; 1541–7.